Biochimica et Biophysica Acta 1792 (2009) 541–547

Contents lists available at ScienceDirect

Biochimica et Biophysica Acta

journal homepage: www.elsevier.com/locate/bbadis

Iron speciation study in *Hfe* knockout mice tissues: Magnetic and ultrastructural characterisation

Lucía Gutiérrez [a,*], Carmen Quintana [b], Cristina Patiño [c], Javier Bueno [c], Hélène Coppin [d,e], Marie P. Roth [d,e], Francisco J. Lázaro [a]

[a] Departamento de Ciencia y Tecnología de Materiales y Fluidos, Universidad de Zaragoza, Centro Politécnico Superior, c/ María de Luna, 3, 50018 Zaragoza, Spain
[b] Instituto de Microelectrónica de Madrid, C.S.I.C., Tres Cantos, 28760 Madrid, Spain
[c] Centro Nacional de Biotecnología, C.S.I.C., Cantoblanco, 28049 Madrid, Spain
[d] INSERM, U563, Centre de Physiopathologie de Toulouse Purpan, Toulouse, F-31300 France
[e] Université Toulouse III Paul-Sabatier, IFR 30, Toulouse, F-31400 France

ARTICLE INFO

Article history:
Received 3 November 2008
Received in revised form 17 March 2009
Accepted 30 March 2009
Available online 5 April 2009

Keywords:
Ferritin
Iron overload diseases
Hfe knockout
Magnetic susceptibility
Biomineralisation

ABSTRACT

Liver, spleen and heart tissues of DBA/2 *Hfe* knockout mice have been characterised by low temperature AC magnetic susceptibility measurements together with Transmission Electron Microscopy (TEM) and Selected Area Electron Diffraction in order to investigate the chemical iron speciation in a murine model of iron overload diseases. With emphasis on ferritin-like species, the temperature dependent in-phase and out-of-phase susceptibility profiles agree with the elemental analysis in that, in this model, iron accumulation takes place in the hepatic tissue while in the spleen and heart tissues no differences have been observed between knockout and wild type animals. The comparison of the magnetic properties between perfused and non-perfused liver tissues has made it possible to estimate the magnetic contribution of usually present blood remains. The TEM observations reveal that, besides the isolated ferritins and ferritin-containing lysosomes–siderosomes present in the hepatocytes, other iron deposits, of heterogeneous size, morphology and crystalline structure (haematite and/or goethite), are present in the cytoplasm, near the membrane, and in extracellular spaces.

1. Introduction

Genetic haemochromatosis is an autosomal recessive disorder characterised by excessive iron absorption from the duodenum and iron release from the macrophages. In humans, gradual deposition of iron occurs in the liver and in a number of other tissues including the pancreas, joints, skin, heart and the gonadotrophin-secreting cells of the anterior pituitary [1,2]. Disease manifestations include hepatic fibrosis, diabetes mellitus, arthropathy, pigmentation, cardiomyopathy and hypogonadotrophic hypogonadism. Liver fibrosis may progress towards cirrhosis, a complication associated with a 200-fold increased risk of hepatocellular carcinoma, the most common cause of death in this condition. Most patients with genetic haemochromatosis are homozygotes for a single point mutation, C282Y, in the *HFE* gene [3]. Population studies have shown that the prevalence of genetic haemochromatosis is one in 300 homozygotes for the C282Y mutation in populations of Northern European extraction.

In the last decades an intense effort has been made in the investigation of the chemical speciation of the tissue iron deposits in cases of iron overload by using Mössbauer spectroscopy [4–10], Transmission Electron Microscopy (TEM) [11–14], infrared spectroscopy [15] and magnetic measurements [16–20], as the biomineralisation of iron in the tissues may be related to its toxicity. In particular, the study of the magnetic properties of these tissues is of special interest to improve non-invasive, magnetism-based, techniques for diagnosis and follow-up treatment of iron overload diseases [21–26].

Murine models of iron overload, like *Hfe* knockout mice ($Hfe^{-/-}$), provide a useful alternative to humans for a better understanding of the physiologic pathways involved in the disease process [27,28]. It has been previously reported that, compared with other mouse strains, DBA/2 mice are particularly susceptible to iron loading in response to *Hfe* disruption [29]. As DBA/2 $Hfe^{-/-}$ mice constitutively become iron overloaded, the model constructed with these animals is expected to be a closer representation of the human disease, at least in terms of genetic origin, than other models like the iron overload induced by parenteral injection of iron dextran.

In this paper, the low temperature AC magnetic susceptibility data of liver, spleen and heart tissues of DBA/2 *Hfe* knockout (KO) and wild type (WT) mice will be presented with the aim of investigating the tissue iron speciation in iron overload diseases. The magnetic results together with elemental analyses and ultrastructural information of the iron deposits, obtained from Transmission Electron Microscopy and Selected Area Electron Diffraction (SAED), will be analysed.

* Corresponding author. Fax: +34976761957.
E-mail address: lucia@unizar.es (L. Gutiérrez).

0925-4439/$ – see front matter © 2009 Elsevier B.V. All rights reserved.
doi:10.1016/j.bbadis.2009.03.007

2. Materials and methods

2.1. Animals

A total of 12 DBA/2 mice, 8 female and 4 male, have been used in this study. Half of the animals were *Hfe* knockout and the rest were wild type, in a way that each KO mice had a WT counterpart of the same age and gender (see Table 1 for details).

All the experiments were performed in accordance with institutional and governmental guidelines and the experimental protocols were approved by the Midi-Pyrénées Animal Ethics Committee. WT and KO mice were housed in the IFR30 animal facility (4–6 animals/cage, 12:12 h light–dark cycle; 22 ± 1 °C, $60 \pm 5\%$ humidity). The animals had free access to R03 diet (UAR, Epinay-sur-Orge, France) containing 280 mg Fe/kg and distilled water.

2.2. Elemental analysis

The animal tissues were analysed by Inductively Coupled Plasma Atomic Emission Spectrometry (ICP-AES) after microwave acid digestion (solution 4:1 (v/v) of HNO_3 (65%) and H_2O_2 (30%)). The magnetically characterised freeze-dried samples (see description below) were subsequently analysed for elemental content in order to allow a quantitative interpretation of the magnetic data. The elemental analysis was focused on the determination of Fe, but the presence of other magnetogenic elements as Co, Ni, Mn and Cu, which may contribute to the magnetic results, was also included in the analysis.

2.3. Transmission electron microscopy

Two different protocols were used for the fixation of the tissues. Half of the animals were sacrificed under pentobarbitone anaesthesia and portions of the livers, spleens and hearts were prepared for TEM observations immediately after tissue dissection. Fragments of the different tissues were fixed for 2 h at room temperature and overnight at 4 °C in a solution of 2% paraformaldehyde (PAF) and 2% glutaraldehyde (Gluta) in 0.1 M phosphate buffer (PB). The rest of the animals were also sacrificed under pentobarbitone anaesthesia although the fixation of the tissues was performed by perfusion. The same fixative (2% PAF, 2% Gluta, 0.1 M PB) was injected directly in the heart and pumped during 8 min at 20 ml/min. Then a different solution containing 0.1 M phosphate buffer was pumped at the same rate during 2 min. A part of the liver was then dissected and left in the fixative at 4 °C overnight.

All the tissues were then postfixed with 1% osmium tetroxide for 45 min at 4 °C. After four washes with buffer, samples were treated with 2% uranyl acetate, dehydrated in graded series of acetone (50, 70, 90, 100%) for 15 min each at 4 °C and embedded in Epon resin at room temperature for 24 h. The polymerisation was done at 60 °C for 48 h.

Ultra-thin sections (40–60 nm) were collected on formvar-coated grids and some of them were also lightly stained with 2% uranyl acetate for 30–60 s or stained with saturated uranyl acetate and lead citrate by standard procedures.

The TEM characterisation was carried out in a Jeol 1010 microscope operated at 100 kV and in a Jeol 1200FX. X-ray microanalysis was also performed with these equipments in order to determine the presence of iron in the tissues.

2.4. AC susceptibility

Samples of the tissues for the magnetic characterisation were prepared as follows. In the case of the non-perfused animals, the spleen, heart and liver tissues were immediately frozen at −80 °C after dissection. These tissues were freeze-dried during 48 h in a Heto PowerDry PL3000 equipment and then ground to powder in order to have a homogeneous sample. The fixed liver samples of the perfused animals were stored at 4 °C, freeze-dried during 24 h in the same equipment and then ground to powder. The powder of each liver sample was placed in individual gelatine capsules for the magnetic measurements.

Due to the small available amount of spleen and heart tissues, pools of samples were prepared for the magnetic characterisation. The spleen tissues of the KO mice (two female and one male) were joined into a single gelatine capsule; doing the same thing with the WT counterparts. The heart tissue samples were prepared following identical procedure.

The magnetic characterisation has been carried out in a Quantum Design MPMS-5S SQUID magnetometer with an AC susceptibility option. The measurements were performed with an AC amplitude of 0.45 mT and at a frequency of 1 Hz in the temperature range 1.8–300 K. The presence of adsorbed oxygen in the samples, which would contribute to the magnetic susceptibility [30], has been checked and avoided by repeated runs above and below its boiling temperature in all the cases.

3. Results

3.1. Elemental analysis

The elemental iron content of each tissue is shown in Table 1. For livers, it varies in a range between 1.729 and 3.903 mg Fe/g dry tissue for KO mice and between 0.371 and 0.636 mg Fe/g dry tissue for the WT ones. For spleen and heart tissues, there are no such big differences in the iron content between the KO and WT tissue pools.

Table 1
Height values of the out-of-phase susceptibility maximum ($\chi''(T)_{max}$) for the different tissue samples, genotype (WT = wild type; KO = knockout), gender (M = male; F = female), age of the animals, elemental iron content and effective moment per iron ion (μ_{eff}).

Animal	Organ	Genotype	Gender	Age (weeks)	Perfusion	$\chi''(T)_{max}$ (m^3/kg)	[Fe] (mg/g)	μ_{eff} (μ_B)
1	Liver	WT	M	9	No	$1.9.10^{-10}$	0.436	2.43
2	Liver	KO	M	9	No	$1.1.10^{-9}$	2.579	2.69
3	Liver	WT	F	9	No	$3.1.10^{-10}$	0.614	2.95
4	Liver	WT	F	9	No	$3.1.10^{-10}$	0.636	2.92
5	Liver	KO	F	9	No	$3.1.10^{-9}$	3.903	3.15
6	Liver	KO	F	9	No	$1.9.10^{-9}$	2.537	3.46
7	Liver	WT	M	14	Yes	$2.4.10^{-10}$	0.439	3.72
8	Liver	KO	M	14	Yes	$2.0.10^{-9}$	1.729	3.23
9	Liver	WT	F	14	Yes	$4.0.10^{-10}$	–	–
10	Liver	KO	F	14	Yes	$2.8.10^{-9}$	2.496	3.28
11	Liver	WT	F	14	Yes	$4.9.10^{-10}$	0.371	3.61
12	Liver	KO	F	14	Yes	$3.0.10^{-9}$	2.764	3.37
1 + 3 + 4	Spleen	WT	2F + 1M	9	No	$8.8.10^{-10}$	1.996	2.18
2 + 5 + 6	Spleen	KO	2F + 1M	9	No	$7.5.10^{-10}$	1.835	2.51
1 + 3 + 4	Heart	WT	2F + 1M	9	No	–	0.450	3.17
2 + 5 + 6	Heart	KO	2F + 1M	9	No	–	0.375	3.44

The $\chi''(T)$ maximum and the iron content are expressed per mass of dry tissue.

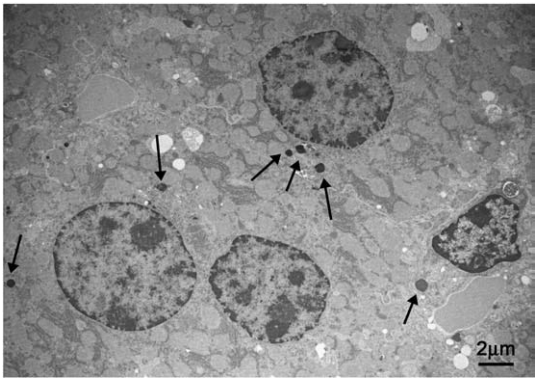

Fig. 1. Liver tissue TEM micrograph of a KO female mouse 9 weeks old. Electron dense iron deposits (marked with arrows) can be observed in the cytoplasm of the hepatocytes.

The content of other magnetogenic elements (Cu, Co, Mn and Ni) is always less than 0.003 wt.% of the freeze-dried tissues.

3.2. Ultrastructural observations

TEM observations of the KO liver tissues show hepatocytes with a dense cytoplasm where the nucleus and all the organelles are well preserved (Fig. 1). In these tissues, in lightly stained sections, several types of electron-dense deposits, in which the presence of iron has been confirmed by X-ray microanalysis, are observed in the cytoplasm of hepatocytes and Kupffer cells and also in intercellular spaces. It is important to note that, in spite of the iron excess in the KO livers, the physiological tissue structure seems not to be altered, as the reported in other animal models of iron overload [18].

Observations at higher magnification (Fig. 2) allow to classify the iron-containing deposits into three types: i) cores of ferritin molecules (1) dispersed in the cytoplasm of cells, sometimes localised near the endoplasmic reticulum (ER), ii) cores of ferritin-haemosiderin molecules (2) in lysosomes–siderosomes of a size that ranges between 0.3 and 0.8 µm and iii) deposits of heterogeneous shape and size (3), observed mainly in the cytoplasm near the membrane and in the extracellular space.

Table 2
Calculated *d* spacings (nm) from the SAED ring data for the different deposits observed in the liver sections.

Six-line Ferrihydrite	Liver iron deposits			Haematite	Goethite
	Type 1 and 2	Type 3			
		0.41			0.418
			0.360	0.368	0.338
			0.260	0.270	0.269
					0.258
0.254	0.253	0.25–0.24		0.252	0.249
					0.245
0.223	0.224	0.22	0.210	0.221	0.219
0.197	0.197				
		0.183		0.184	
					0.172
0.172	0.170	0.170	0.171	0.169	0.169
					0.156
					0.151
0.151	0.147	0.147	0.147	0.149	0.147
0.147	0.145	0.145		0.145	0.145

Deposits type 1 and 2 correspond to isolated spherical particles and lysosomes–siderosomes containing spherical electron-dense particles respectively, while type 3 correspond to the very electron-dense deposits shown in Fig. 2 (the two data columns in this group correspond to two different occurrences of this type of deposits). For comparison, the corresponding values for ferrihydrite (a = b = 0.508 nm, c = 0.94 nm), haematite (a = b = 0.503 nm, c = 1.37 nm) and goethite (a = 0.461, b = 0.996 nm, c = 0.302 nm) [36] are indicated.

Selected Area Electron Diffraction (SAED) performed on deposits type 1 and 2 show a mineralisation similar to ferrihydrite (Table 2), the most common mineral found in physiological ferritin cores [31,32]. A set of rings, different from those of ferrihydrite and consistent with haematite and/or goethite phases, appear in the diffraction pattern of type 3 deposits (Table 2), although a deeper study on their nature is still needed.

3.3. AC magnetic susceptibility

The temperature dependence of the AC susceptibility per mass of sample of mice liver tissues is shown in Figs. 3 and 4. For the sake of

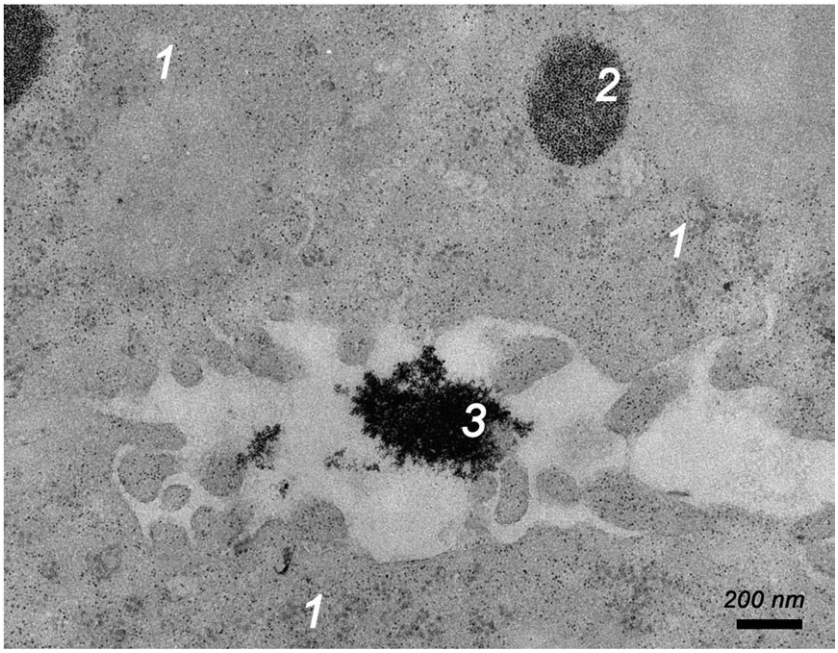

Fig. 2. TEM micrograph at higher magnification of the same liver tissue shown in Fig. 1 corresponding to a KO female mouse. Isolated spherical particles typical of ferritin (1), and lysosomes–siderosomes containing spherical electron-dense particles (2) can be observed in the cytoplasm of the hepatocytes, while very electron-dense deposits (3) are visible in the extracellular space.

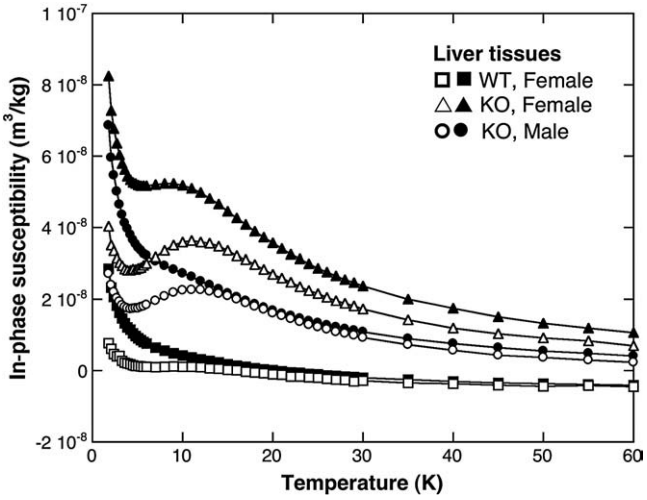

Fig. 3. Temperature dependence of the in-phase susceptibility $\chi'(T)$, at 1 Hz, per mass of freeze-dried liver tissue corresponding to mice of different gender and genotype, some of them subjected to perfusion. Filled symbols correspond to non-perfused animals and empty symbols to the perfused ones.

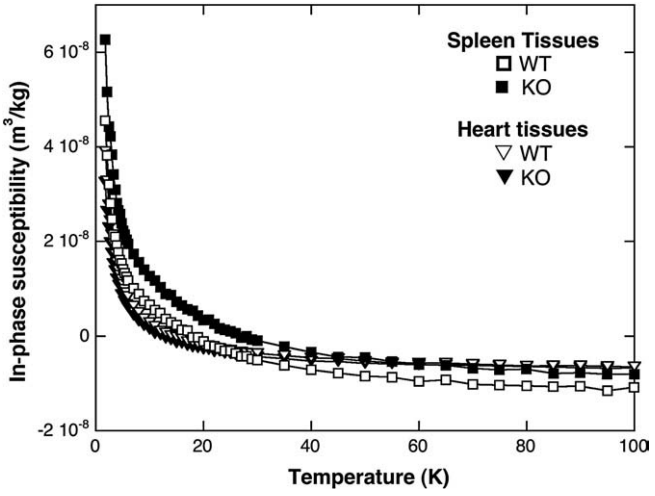

Fig. 5. Temperature dependence of the in-phase susceptibility $\chi'(T)$, at 1 Hz, per mass of freeze-dried tissues of the spleen and heart tissue pools corresponding to mice of different genotype.

clarity only the results from six animals are shown in the graphs, although data from all the characterised tissues have been listed in Table 1.

A low temperature paramagnetic tail can be observed in the in-phase susceptibility $\chi'(T)$ of all the liver samples. The in-phase component of some of the samples also shows a maximum, or a small shoulder, around 11 K that, together with the non-zero out-of-phase susceptibility $\chi''(T)$ at the same temperature range, provide evidence for a magnetic relaxation phenomenon. The out-of-phase susceptibility of all the liver tissues shows a single maximum around 8 K and stays negligible, within the accuracy of the experiments, above approximately 25 K reminding previous results obtained for rat liver ferritin [18]. The value of the susceptibility per mass of sample of the out-of-phase maxima of all the samples is shown in Table 1.

The spleen and heart pools of the KO and WT animals present a low temperature paramagnetic tail in the in-phase susceptibility in all the cases (Fig. 5). The out-of-phase susceptibility of the corresponding four samples is plotted in Fig 6. It can be observed that the heart samples show a nearly negligible out-of-phase susceptibility in all the temperature range, while a small and rather noisy maximum at low temperatures can be observed for the spleen samples. For both tissues, the susceptibility results do not show significant differences between the KO and the WT animals.

4. Discussion

From the data in Table 1, it can be observed that the KO animals have, as expected, a greater concentration of iron in the liver tissue than the WT ones. No significant differences are observed between 9 and 14 week old animals, in agreement with unpublished observations indicating that the hepatic iron concentration in $Hfe^{-/-}$ mice increases sharply after weaning but stabilises after few weeks. Besides, the iron contents of the KO mice tissues obtained from the elemental analysis are also similar to those previously determined by biochemical methods in the same animal model of iron overload [29].

Although their protein shell is not visible in these TEM micrographs, a large amount of ferritin cores can be observed in the cytoplasm. The actual presence of the ferritin molecules is evidenced from the shape (approximately spherical) and the size (not larger than about 8 nm) of their electron-dense cores that, besides, in lightly stained sections, appear mutually separated by the non-electron-

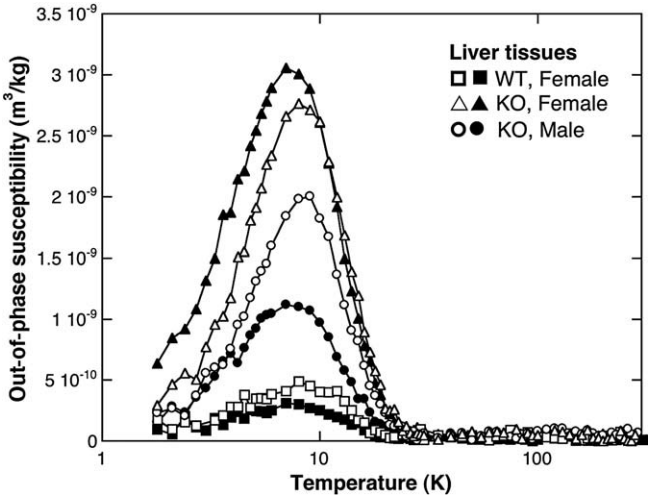

Fig. 4. Temperature dependence of the out-of-phase susceptibility $\chi''(T)$, at 1 Hz, per mass of freeze-dried liver tissue corresponding to mice of different gender and genotype, some of them subjected to perfusion. Filled symbols correspond to non-perfused animals and open symbols to the perfused ones.

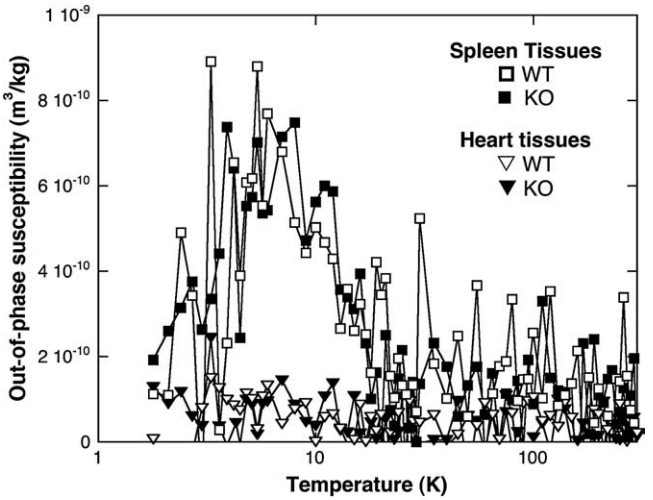

Fig. 6. Temperature dependence of the out-of-phase susceptibility $\chi''(T)$, at 1 Hz, per mass of freeze-dried tissues of the spleen and heart tissue pools corresponding to mice of different genotype.

dense protein shells [13]. The presence of ferritin molecules near the ER may indicate a profuse synthesis of this protein in the liver tissues.

The size and shape of the iron-containing particles inside the lysosomes–siderosomes is similar to those of the ferritin cores. However, the apparent mutual contact between them may indicate that the protein shell has undergone a certain degradation, analogously to what has been observed in the so-called secondary lysosomes [33,13]. This type of deposit has been mentioned in the degradation sequence of ferritin, in the lysosomes, to form haemosiderin [12,14]. In fact some authors have called them "prehaemosiderin", indicating that the mineral cores would not be altered yet [5]. In addition, it has to be taken into account that when observing closed packed ferritin particles in structures such as these lysosomes, mineral particles may appear to be in contact even if the protein shell is intact. However, independently of the term used to describe these clusters or the state of the protein shell, it is clear that they contain a large part of the total iron accumulated in the liver.

The intracellular and extracellular type 3 iron deposits observed in the micrographs show neither morphological nor crystalline similarities with the ferritin cores. Their location near the membranes and in the extracellular space may indicate a process of iron removal from the cell, possibly explaining why the tissues are relatively well preserved in spite of the iron excess. In fact, the beneficial role of biomineralisation processes in preventing iron toxicity has been pointed out in relation to the formation of haemosiderin [34]. Goethite deposits in tissues have previously been observed in conditions of iron overload [6,7,34], while haematite, as far as we know, has only been mentioned as a minor phase in physiological ferritin cores [32,35]. It is therefore in this work, in our opinion, the first time that the presence of haematite-like deposits are detected in iron overload situations.

As previous studies have reported the transformation from ferrihydrite either to haematite or to goethite, we can hypothesise that our type 3 deposits may be originated from the ferritin ferrihydrite cores. However, while it is known that haematite can be formed from the dehydration of ferrihydrite, the formation of goethite from ferrihydrite would imply its dissolution and further nucleation [36].

As other authors have reported the transformation from ferrihydrite to other iron oxide structures by the effect of the electron beam [37], we have done dedicated experiments to assure that the crystalline structure of type 3 deposits is not due to such effect. In our case, the SAED patterns of ferrihydrite deposits have not been altered after several minutes of irradiation.

From previous works on the study of homologous tissues in rats [18] and from available AC magnetic susceptibility data of ferritin

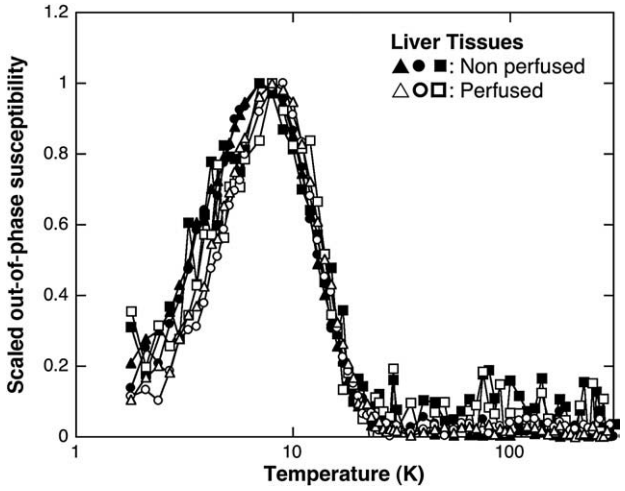

Fig. 7. Comparative plot of the $\chi''(T)$ profiles, scaled to their respective maxima, for the magnetically characterised liver tissues.

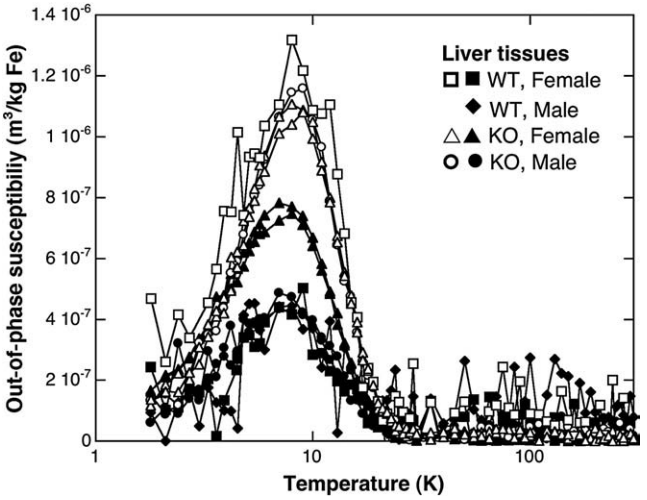

Fig. 8. Temperature dependence of the out-of-phase susceptibility $\chi''(T)$, at 1 Hz, per mass of elemental iron for the liver tissues. Filled symbols correspond to non-perfused animals and open symbols to the perfused ones.

standards [16,18,38], the $\chi''(T)$ maximum observed in these mice tissues can be assigned to the presence of ferritin or, alternatively, to the cores of partially degraded ferritin whose crystalline structure and size are still similar to those of ordinary ferritin. However, the $\chi''(T)$ maxima of the mice tissues are located at slightly lower temperatures (7–9 K) than those previously observed for rat liver ferritin (8–12 K) [18] measured in the same conditions; a phenomenon that may result from small differences in the size of the iron-containing crystallites inside the ferritin cages or from a qualitative different biomineralisation between the two animal genera.

With respect to the contribution of type 3 deposits to the total magnetic susceptibility of the tissues, we expect it to be under the detection limits of the magnetic characterisation. This assumption is based (i) on the fact that these aggregates are quite sparse in the volume in comparison with the ferritin cores and (ii) on the relatively large size of these deposits that, given the antiferromagnetic character of haematite and goethite, result in smaller magnetic moments per iron ion.

When plotting the out-of-phase susceptibility per mass of sample, the height of the $\chi''(T)$ maximum (see data in Fig. 4 only for selected samples and in Table 1 for all of them) informs about the amount of iron in the form of ferritin cores. In Fig. 4, it can be observed that, independently on whether the animals were perfused or not, the $\chi''(T)$ maxima for the KO mice are always higher than for their WT counterparts. This result indicates that the genetically provoked iron overload consists of, not only a greater amount of total iron, but a greater amount of iron in the form of ferritin.

In order to study the differences in shape, width and location of the $\chi''(T)$ maxima it is usually adequate to scale the curves to their maximum height. In Fig. 7 it can be observed that there is a rather good coincidence of the $\chi''(T)$ profile for all the liver samples (perfused and non-perfused, WT and KO) suggesting that in all these cases a very similar biomineralisation, in terms of the formed iron (oxyhydr)oxide, may exist. However, when looking in more detail, it can be observed that, while the high temperature flank of the $\chi''(T)$ profile very well coincides in all the cases, likely due to the size limitation of the ferritin cavity, there are significant differences in the low temperature flank between perfused and non-perfused animals. This result would indicate that, assuming a similar biomineralisation in all the cases, the size distribution of the iron-containing crystallites in the case of the non-perfused animals is more extended to small sizes than in the case of the perfused ones.

Although, as mentioned, no big differences between the $\chi''(T)$ data for perfused and non-perfused animals, of the same genotype and

gender, are observed, they do differ in the in-phase component. The low temperature tail observed in $\chi'(T)$ originates at paramagnetic iron-containing species, that is, molecules or microscopical entities in which the iron atoms may be either bounded to organic ligands (e.g. deoxyhaemoglobin, transferrin) or not, but never in the form of iron (oxyhydr)oxide nanoparticles. This paramagnetic contribution may correspond either to intracellular iron-containing species or to other substances remaining in the blood vessels. The observed $\chi'(T)$ data for the non-perfused animals, independently of gender and genotype, always present a much greater paramagnetic contribution than for the perfused ones. This result appears logical because in the perfusion process the fixative is introduced through the blood vessels – the iron-containing species from the blood are substantially removed – reducing their paramagnetic contribution.

Within a deeper analysis of the iron speciation in the liver tissues, the $\chi''(T)$ data, expressed per mass of iron, are shown in Fig. 8. In this type of representation, if all of the iron atoms in a given tissue were present in the form of a single iron-containing species (e.g. ferritin in this case), the corresponding $\chi''(T)$ data, *per mass of iron*, would coincide with that of isolated ferritin. However, the variable presence of other species not contributing to χ'', like paramagnetic iron, diamagnetic iron, or other weakly magnetic forms of iron as the invoked haematite and/or goethite deposits, will result in that the greater the ratio $Fe_{ferritin}/Fe_{total}$, the higher the $\chi''(T)$ ferritin profile when represented per mass of iron. In particular, in Fig. 8, the $\chi''(T)$ data points for perfused animals significantly appear higher than for the non-perfused ones, meaning that the first ones contain a bigger proportion of ferritin iron. The previously discussed observation of a smaller paramagnetic component in perfused animal tissues (see Fig. 3) independently of their gender or genotype, as it clearly implies removal of iron ions is also consistent with the same idea. It is also worth noting that the height of the $\chi''(T)$ maxima per mass of iron for the perfused mice livers is very similar in all the cases. This coincidence means that the $Fe_{ferritin}/Fe_{total}$ ratio is similar for all those samples in spite of their different iron contents. Within the group of the non-perfused liver tissues, it can be observed that the KO females present a higher iron-specific out-of-phase susceptibility maximum in comparison with their WT counterparts explained by a higher $Fe_{ferritin}/Fe_{total}$ ratio, due to the iron loading. However, the biological explanation of the fact that the iron-specific out-of-phase susceptibility maximum of the KO non-perfused male has the same height as its WT counterparts is not clear for us yet.

The χ'' maximum for spleen tissues (Fig. 6), although more noisy, is located at similar temperatures as liver tissues, most likely corresponding also to ferritin iron. For heart tissues, $\chi''(T)$ is nearly negligible in all the temperature range meaning that the detection of ferritin iron in these samples is beyond the limits of the technique. For both spleen and heart tissues, the susceptibility of the pool samples in the case of KO animals does not differ significantly from the WT ones indicating that there is no particular iron accumulation in these tissues, in agreement with the determined elemental iron contents (Table 1).

The magnetic data in this mouse model of iron overload can be compared with the rat model constructed by means of a single injection of iron dextran [17–19]. In that model iron deposits were observed in liver, spleen, muscle, heart and kidney tissues while in the present case of DBA/2 *Hfe* KO mice iron overload it has only been observed in the liver.

For all the studied tissues, in the high temperature range, $\chi'(T)$ show Curie-type behaviour as it is typical for a paramagnet, a superparamagnet, or a mixture of both. As it has been previously explained [17], the high temperature paramagnetic and superparamagnetic contributions are mixed up on a single Curie-law susceptibility whose information is condensed into the value of the effective moment μ_{eff} per iron ion (for a deeper explanation of the calculation of the μ_{eff} value of tissue samples see ref. [17]). As each iron-containing species usually has a characteristic effective moment per iron ion, namely, 5.46 μ_B for deoxyhaemoglobin, 0 μ_B for oxyhaemoglobin and 3.4 μ_B for ferritin [39–41,18], the effective moment per iron ion determined for the whole tissue sample results from the average of the μ_{eff} values, weighted with the relative abundances of each species.

The effective moments per iron ion of all the characterised samples are shown in Table 1. It can be seen that $\mu_{eff} = 2.93 \pm 0.36$ (mean + s.d.) in the case of non-perfused animals and 3.23 ± 0.17 for the perfused ones. This significant result may indicate that the iron removed in the perfusion process, although being in part of paramagnetic nature, may include an important content of low magnetic moment iron, which may be of diamagnetic and/or antiferromagnetic (large particle size) nature.

5. Conclusions

In this work, for the first time, AC magnetic susceptibility measurements together with TEM analysis have been used to study the iron deposits formed in the tissues of DBA/2 *Hfe* KO mice.

No differences between KO and WT mice have been observed in the iron content of spleen and heart tissues. However, an increased iron accumulation in liver tissues has been found for the KO mice.

The differences in shape and location of the $\chi''(T)$ maxima, corresponding to the ferritin cores contribution, observed between different animal genera (data of these mice and previous data for rats [18]) may indicate a slightly different qualitative biomineralisation or different size distribution of the iron-containing crystallites.

The perfusion procedure has revealed that a considerable part of the paramagnetic contribution observed in the non-perfused tissues comes from iron-containing species in the remaining blood.

Iron deposits whose morphology, size and crystalline structure (haematite and/or goethite) appear different from those of ferritin and those of lysosomes–siderosomes containing ferritin-haemosiderin have been observed in the liver tissues by TEM and SAED analysis. This finding deserves a more detailed study, as it may be related to the apparently healthy aspect of the tissues, and opens the way to future studies on biomineralisation processes in cases of iron overload and related to potential treatments of the disease. The formation of these iron-containing deposits may be a way to avoid free iron and the oxidative stress related to it.

The combination of magnetic characterisation and TEM analysis has been proven to be of great usefulness to study the nature and the evolution of tissue iron deposits in conditions of iron overload.

Acknowledgements

We thank Ana Rosa Abadía, Laure Verret and Claire Rampon for technical support. Financial support from Instituto de Salud Carlos III through project PI060549 is acknowledged. Lucía Gutiérrez thanks Gobierno de Aragón and Fondo Social Europeo for Grant B091/2005.

We are also very grateful to the anonymous referees for having generously given their time in helping us to improve this manuscript.

References

[1] N.C. Andrews, Disorders of iron metabolism, N. Engl. J. Med. 341 (1999) 1986–1995.
[2] A. Pietrangelo, Hereditary hemochromatosis—a new look at an old disease, N. Engl. J. Med. 350 (2004) 2383.
[3] J.N. Feder, A. Gnirke, W. Thomas, Z. Tsuchihashi, D.A. Ruddy, A. Basava, F. Dormishian, R. Domingo, M.C. Ellis, A. Fullan, A novel MHC class I-like gene is mutated in patients with hereditary haemochromatosis, Nat. Genet. 13 (1996) 399–408.
[4] S.C. Andrews, M.C. Brady, A. Treffry, J.M. Williams, S. Mann, M.I. Cleton, W. de Bruijn, P.M. Harrison, Studies on haemosiderin and ferritin from iron-loaded rat liver, Biol. Met. 1 (1988) 33–42.
[5] T.G. St. Pierre, D.P.E. Dickson, J.K. Kirkwood, R.J. Ward, T.J. Peters, A Mössbauer spectroscopic study of the form of iron in iron overload, Biochim. Biophys. Acta 924 (1987) 447–451.

[6] T.G. St. Pierre, K.C. Tran, J. Webb, D.J. Macey, P. Pootrakul, D.P.E. Dickson, Core structures of haemosiderins deposited in various organs in beta-thalassemia hemoglobin-E disease, Hyperfine Interact. 71 (1992) 1279–1282.
[7] T.G. St Pierre, W. Chua-anusorn, J. Webb, D. Macey, P. Pootrakul, The form of iron oxide deposits in thalassemic tissues varies between different groups of patients: a comparison between Thai beta-thalassemia/hemoglobin E patients and Australian beta-thalassemia patients, Biochim. Biophys. Acta, Mol. Basis Dis. 1407 (1998) 51–60.
[8] T.G. St. Pierre, W. Chua-anusorn, J. Webb, D.J. Macey, Iron overload diseases: the chemical speciation of non-heme iron deposits in iron loaded mammalian tissues, Hyperfine Interact. 126 (2000) 75–81.
[9] R.J. Ward, M. Ramsey, D.P.E. Dickson, C. Hunt, T. Douglas, S. Mann, F. Aouad, T.J. Peters, R.R. Crichton, Further characterization of forms of hemosiderin in iron-overloaded tissues, Eur. J. Biochem. 225 (1994) 187–194.
[10] J. Webb, T.G. St. Pierre, K.C. Tran, W. Chua-anusorn, D.J. Macey, P. Pootrakul, Biologically significant iron(III) oxyhydroxy polymers: Mössbauer spectroscopic study of ferritin and hemosiderin in pancreas tissue of beta-thalassemia hemoglobin E disease, Inorg. Chim. Acta 243 (1996) 121–125.
[11] G.W. Richter, The cellular transformation of injected colloidal iron complexes into ferritin and hemosiderin in experimental animals — a study with the aid of electron microscopy, J. Exp. Med. 109 (1959) 197–233.
[12] G.W. Richter, Studies of iron overload. Rat liver siderosome ferritin, Lab. Invest. 50 (1984) 26–35.
[13] T.C. Iancu, Ferritin and hemosiderin in pathological tissues, Electron Microsc. Rev. 5 (1992) 209–229.
[14] T.C. Iancu, Y. Deugnier, J.W. Halliday, L.W. Powell, P. Brissot, Ultrastructural sequences during liver iron overload in genetic hemochromatosis, J. Hepatol. 27 (1997) 628–638.
[15] W. Chua-anusorn, K.C. Tran, J. Webb, D.J. Macey, T.G. St Pierre, Chemical speciation of iron deposits in thalassemic heart tissue, Inorg. Chim. Acta 300 (2000) 932–936.
[16] P.D. Allen, T.G. St. Pierre, W. Chua-anusorn, V. Strom, K.V. Rao, Low-frequency low-field magnetic susceptibility of ferritin and hemosiderin, Biochim. Biophys. Acta, Mol. Basis Dis. 1500 (2000) 186–196.
[17] F.J. Lázaro, A.R. Abadía, M.S. Romero, L. Gutiérrez, J. Lázaro, M.P. Morales, Magnetic characterisation of rat muscle tissues after subcutaneous iron dextran injection, Biochim. Biophys. Acta, Mol. Basis Dis. 1740 (2005) 434–445.
[18] L. Gutiérrez, F.J. Lázaro, A.R. Abadía, M.S. Romero, C. Quintana, M.P. Morales, C. Patiño, R. Arranz, Bioinorganic transformations of liver iron deposits observed by tissue magnetic characterisation in a rat model, J. Inorg. Biochem. 100 (2006) 1790–1799.
[19] F.J. Lázaro, L. Gutiérrez, A.R. Abadía, M.S. Romero, A. López, Biological tissue magnetism in the frame of iron overload diseases, J. Magn. Magn. Mater. 316 (2007) 126–131.
[20] S. Hackett, W. Chua-anusorn, P. Pootrakul, T.G. St. Pierre, The magnetic susceptibilities of iron deposits in thalassaemic spleen tissue, Biochim. Biophys. Acta, Mol. Basis Dis. 1772 (2007) 330–337.
[21] G.M. Brittenham, D.G. Badman, Noninvasive measurement of iron: report of an NIDDK workshop, Blood 101 (2003) 15–19.
[22] G.M. Brittenham, D.E. Farrell, J.W. Harris, E.S. Feldman, E.H. Danish, W.A. Muir, J.H. Tripp, E.M. Bellon, Magnetic susceptibility measurement of human iron stores, N. Engl. J. Med. 307 (1982) 1671–1675.
[23] P. Nielsen, R. Engelhardt, J. Dullmann, R. Fischer, Non-invasive liver iron quantification by SQUID-biosusceptometry and serum ferritin iron as new diagnostic parameters in hereditary hemochromatosis, Blood Cells Mol. Dis. 29 (2002) 451–458.
[24] P.D. Jensen, Evaluation of iron overload, Br. J. Haematol. 124 (2004) 697–711.
[25] Y. Gandon, D. Olivie, D. Guyader, C. Aube, F. Oberti, V. Sebille, Y. Deugnier, Non-invasive assessment of hepatic iron stores by MRI, Lancet 363 (2004) 357–362.
[26] T.G. St. Pierre, P.R. Clark, W. Chua-anusorn, A.J. Fleming, G.P. Jeffrey, J.K. Olynyk, P. Pootrakul, E. Robins, R. Lindeman, Noninvasive measurement and imaging of liver iron concentrations using proton magnetic resonance, Blood 105 (2005) 855–861.
[27] X.Y. Zhou, S. Tomatsu, R.E. Fleming, S. Parkkila, A. Waheed, J. Jiang, Y. Fei, E.M. Brunt, D.A. Ruddy, C.E. Prass, *HFE* gene knockout produces mouse model of hereditary hemochromatosis, Proc. Nat. Acad. Sci. U. S. A. 95 (1998) 2492–2497.
[28] S. Bahram, S. Gilfillan, L.C. Kuhn, R. Moret, J.B. Schulze, A. Lebeau, K. Schumann, Experimental hemochromatosis due to MHC class I HFE deficiency: immune status and iron metabolism, Proc. Nat. Acad. Sci. U. S. A. 96 (1999) 13312–13317.
[29] F. Dupic, S. Fruchon, M. Bensaid, N. Borot, M. Radosavljevic, O. Loréal, P. Brissot, S. Gilfillan, S. Bahram, H. Coppin, Inactivation of the hemochromatosis gene differentially regulates duodenal expression of iron-related mRNAs between mouse strains, Gastroenterology 122 (2002) 745–751.
[30] H. Kanoh, K. Kaneko, Magnetic spin states of O_2 confined in a graphitic slit-shaped nanospace at low temperature, J. Phys. Chem. 100 (1996) 755–759.
[31] K. Towe, W. Bradley, Mineralogical constitution of colloidal 'hydrous ferric oxides', J. Colloid Interface Sci. 24 (1967) 348–392.
[32] J.M. Cowley, D.E. Janney, R.C. Gerkin, P.R. Buseck, The structure of ferritin cores determined by electron nanodiffraction, J. Struct. Biol. 131 (2000) 210–216.
[33] P.M. Harrison, P. Arosio, Ferritins: molecular properties, iron storage function and cellular regulation, Biochim. Biophys. Acta, Bioenerg. 1275 (1996) 161–203.
[34] R.J. Ward, R. Legssyer, C. Henry, R.R. Crichton, Does the haemosiderin iron core determine its potential for chelation and the development of iron-induced tissue damage? J. Inorg. Biochem. 79 (2000) 311–317.
[35] C. Quintana, J.M. Cowley, C. Marhic, Electron nanodiffraction and high-resolution electron microscopy studies of the structure and composition of physiological and pathological ferritin, J. Struct. Biol. 147 (2004) 166–178.
[36] R.M. Cornell, U. Schwertmann, The Iron Oxides: Structure, Properties, Reactions, occurrences and uses, Wiley-VCH, 1996.
[37] Y. Pan, A. Brown, R. Brydson, A. Warley, A. Li, J. Powell, Electron beam damage studies of synthetic 6-line ferrihydrite and ferritin molecule cores within a human liver biopsy, Micron 37 (2006) 403–411.
[38] F. Luis, E. del Barco, J.M. Hernández, E. Remiro, J. Bartolomé, J. Tejada, Resonant spin tunneling in small antiferromagnetic particles, Phys. Rev. B: Condens. Matter 59 (1999) 11837–11846.
[39] L. Pauling, C.D. Coryell, The magnetic properties and structure of hemoglobin, oxyhemoglobin and carbonmonoxyhemoglobin, Proc. Nat. Acad. Sci. U. S. A. 22 (1936) 210–216.
[40] Y. Alpert, R. Banerjee, Magnetic susceptibility measurements of deoxygenated hemoglobins and isolated chains, Biochim. Biophys. Acta 405 (1975) 144–154.
[41] L. Pauling, Magnetic properties and structure of oxyhemoglobin, Proc. Nat. Acad. Sci. U. S. A. 74 (1977) 2612–2613.